

Magnetic Collective Mode Dispersion in High Temperature Superconductors

M. R. Norman

Materials Science Division, Argonne National Laboratory, Argonne, IL 60439

Recent neutron scattering experiments in the superconducting state of YBCO have been interpreted in terms of a magnetic collective mode whose dispersion relative to the commensurate wavevector has a curvature opposite in sign to a conventional magnon dispersion. The purpose of this article is to demonstrate that simple linear response calculations are in support of a collective mode interpretation, and to explain why the dispersion has the curvature it does.

PACS numbers: 25.40.Fq, 71.18.+y, 74.25.Jb, 74.72.-h

Inelastic neutron scattering, which measures the momentum and energy dependence of the dynamic spin susceptibility, has emerged as a powerful probe of high temperature cuprate superconductors¹. One of the most striking features of the data is the appearance below the superconducting transition temperature of a commensurate resonance in the case of the bilayer cuprates, YBCO and Bi₂212²⁻⁵. In addition, an incommensurate magnetic response has been seen for energies below the resonance energy in both cases⁶⁻⁸. Recently, it has been argued that these two structures are part of the same collective mode dispersion⁹. This interpretation is unusual in that the curvature of the purported collective mode dispersion relative to the commensurate wavevector is opposite in sign to that of a conventional magnon dispersion.

One of the motivations of this interpretation is the similarity of the measured dispersion to theoretical results based on linear response theory (RPA)¹⁰⁻¹⁴. In these works, though, it was unclear whether the incommensurate response below resonance was actually due to a pole in the response function as would be expected for a collective mode interpretation. The purpose of this article is to investigate this issue in detail.

The methodology is standard, and details can be found in Ref. 14. An effective quasiparticle dispersion is used to calculate the bare bubble in the superconducting state, χ_0 . The RPA susceptibility is then obtained as $\chi_0/(1 - J\chi_0)$. The most crucial input is the form of the dispersion. In Ref. 14, two dispersions were analyzed, one based on angle resolved photoemission (ARPES) data in the normal state (tb1), another on ARPES data in the superconducting state where the Fermi surface was flattened around the node to enhance the effects of incommensurability (tb2). In addition, in this paper, a slight modification of this second dispersion was made to further enhance the incommensurability (tb3). All three dispersions are listed in Table I for completeness sake. For the superconducting gap, the standard $\cos(k_x) - \cos(k_y)$ form was assumed, with a maximum value, Δ_{max} , taken from recent tunneling measurements in YBCO¹⁵. J was adjusted to obtain a resonance at 41 meV, the resulting J being similar in value to estimates based on neutron

scattering in underdoped samples¹⁶.

To begin, it is helpful to discuss the frequency dependence of the bare bubble, χ_0 . In Figure 1, $Re\chi_0$ and $Im\chi_0$ are shown at a typical incommensurate wavevector for the three dispersions of Table 1. In $Im\chi_0$, there are two steps, a low energy one at threshold, and another at slightly higher energy. The two energies correspond to the spin gap energies $\omega_g(\pm q) = \min_k(E_k + E_{k\pm q})$, where k is confined to the first quadrant of the Brillouin zone and E_k are the quasiparticle energies in the superconducting state. The steps are a consequence of the coherence factors associated with a d-wave order parameter. For the commensurate wavevector, $Q = (\pi, \pi)$, these two energies are degenerate, so there is only one step. By the Kramers-Kronig relations, these steps lead to logarithmic divergences in $Re\chi_0$ which become simple peaks when damping is taken into account. (All plotted results are obtained by replacing ω by $\omega + i\Gamma$ in the energy denominators when calculating χ_0).

In Figure 2, $Re\chi_0$ and $Im\chi_0$ are shown as a function of q at an energy of 35 meV for the three dispersions of Table 1. In the first case (tb1), one finds the typical result that $Re\chi_0$ is quadratic relative to the commensurate wavevector Q with a negative curvature (i.e., a maximum at Q). Since $Re\chi_0$ increases with ω (up to the spin gap energy $\omega_g(Q)$), one expects that the RPA pole condition, $1 - JRe\chi_0 = 0$, will be satisfied first at Q , then at higher energies at wavevectors increasingly displaced from Q . This would then give a conventional magnon like dispersion. The actual situation is more complicated, though. Note in Figure 2a that there is a second maximum in $Re\chi_0$ at an incommensurate wavevector, associated with $\omega_g(q)$ as discussed in the context of Figure 1. As the energy increases, this second maximum becomes the global maximum.

In Figure 3a, the q vector where the RPA $Im\chi$ is maximal at a given ω ($\omega(q)$) is plotted for this dispersion. In agreement with experiment, one finds incommensurability below the resonance energy, but the RPA pole condition is not satisfied below resonance. Instead the incommensurability simply tracks $\omega_g(q)$. As a consequence, the intensity plummets below resonance, as can be seen in Figure 4a. Above resonance, the RPA pole condition

is satisfied, but as can be seen in Figure 3a, the dispersion crosses into the continuum (i.e., beyond $\omega_g(q)$) just above resonance, so the mode becomes damped, as obvious from the intensity plot of Figure 4a.

The above behavior is not what is observed, in that the experimental intensity decays more slowly below resonance. This is because the incommensurability effects associated with dispersion tb1 are too weak. This can be contrasted with the dispersion analyzed by Brinkmann and Lee¹⁰. In that case, the constant energy contours of E_k are quite flat for energies below Δ_{max} , leading to an enhancement in the incommensurate effects. This can be seen in Figures 2b and 2c, where $Re\chi_0$ is plotted for the other two dispersions considered here (tb2 and tb3). In the first case (tb2), the dispersion used in earlier work¹⁴, one finds a rather flat behavior around Q due to the flat quasiparticle dispersion around $k = (\pi, 0)$. In addition, a global maximum now occurs at an incommensurate wavevector due to the flattening of the Fermi surface around the d-wave nodal (π, π) directions relative to dispersion tb1.

The resulting dispersion, $\omega(q)$, of $Im\chi$ from tb2 is plotted in Figure 3b. This is in better agreement with experimental results in YBCO^{8,9}. In addition, it can be seen from this plot that the RPA pole condition is now satisfied below the resonance energy for a few meV until the spin gap energy, $\omega_g(q)$, is encountered. For energies below this, the mode is strongly diminished in intensity as it traces out the edge of the continuum. This result is consistent with earlier work¹².

Although Figure 3b is in good agreement with experiment as far as $\omega(q)$ is concerned, it is still deficient in that the intensity of $Im\chi$ below resonance still drops off faster than experiment, as plotted in Figure 4b and also noted earlier¹⁴. To analyze this further, dispersion tb2 was modified by making the dispersion less flat in one direction around $(\pi, 0)$, and flattening the Fermi surface around the d-wave node even more. The resulting $Re\chi_0$ is shown in Figure 2c, and is similar to that obtained earlier by Brinkmann and Lee¹⁰. One now finds a truly quadratic behavior around Q with positive curvature, a direct consequence of the stronger incommensurate peaks. As a consequence, the RPA pole condition is satisfied for an even greater energy range below resonance (Figure 3c), and moreover, the intensity below resonance falls off much more slowly (Figure 4c), as observed experimentally.

The results in this paper concentrated on the (π, q_y) direction, since this is where the maximum in the incommensurability was observed. Two dimensional q plots from dispersions tb2 and tb3 are consistent with experiment⁶ in showing a baseball diamond shaped incommensurability pattern below resonance with global maxima along (π, q_y) and (q_x, π) , as reported earlier¹⁴. Recently, an anisotropy was observed in this intensity pattern for partially detwinned YBCO samples¹⁷. If this is a true magnetic anisotropy not related to the phonon background, then within the RPA context, it would have

to be due to the influence of the chain bands wiping out two of the incommensurate spots, not surprising given the sensitivity of the incommensurability to the electronic structure. On the other hand, this is conjecture at this stage, as a proper calculation taking into account both plane and chain bands has yet to be performed. Of course, the most natural explanation of this anisotropy would be due to stripe formation, but it is unclear whether such a picture can reproduce the results demonstrated here (in particular, the energy dependence of the incommensurability).

In conclusion, RPA calculations of the dynamic susceptibility are in support of a collective mode interpretation of the magnetic dispersion relation observed in bilayer cuprate superconductors. The observed incommensurability has strong implications for the effective quasiparticle dispersion, and it would be of interest to verify whether the dispersions analyzed here, in particular in regards to the flattening of the Fermi surface around the d-wave node, are consistent with high resolution angle resolved photoemission data, particularly in the case of YBCO.

The author thanks Andrei Chubukov and Oleg Tchernyshyov for discussions. This work was supported by the U.S. Dept. of Energy, Basic Energy Sciences, under Contract No. W-31-109-ENG-38.

¹ H. F. Fong, P. Bourges, Y. Sidis, L. P. Regnault, J. Bossy, A. Ivanov, D. L. Milius, I. A. Aksay, and B. Keimer, Phys. Rev. B **61**, 14773 (2000).

² J. Rossat-Mignod, L. P. Regnault, C. Vettier, P. Bourges, P. Burlet, J. Bossy, J. Y. Henry, and G. Lapertot, Physica C **185-189**, 86 (1991).

³ H. A. Mook, M. Yethiraj, G. Aeppli, T. E. Mason, and T. Armstrong, Phys. Rev. Lett. **70**, 3490 (1993).

⁴ H. F. Fong, B. Keimer, P. W. Anderson, D. Reznik, F. Dogan, and I. A. Aksay, Phys. Rev. Lett. **75**, 316 (1995).

⁵ H. F. Fong, P. Bourges, Y. Sidis, L. P. Regnault, A. Ivanov, G. D. Gu, N. Koshizuka, and B. Keimer, Nature **398**, 588 (1999).

⁶ H. A. Mook, P. Dai, S. M. Hayden, G. Aeppli, T. G. Perring, and F. Dogan, Nature **395**, 580 (1998).

⁷ H. A. Mook, F. Dogan, and B. C. Chakoumakos, preprint cond-mat/9811100.

⁸ M. Arai, T. Nishijima, Y. Endoh, T. Egami, S. Tajima, K. Tomimoto, Y. Shiohara, M. Takahashi, A. Garrett, and S. M. Bennington, Phys. Rev. Lett. **83**, 608 (1999).

⁹ P. Bourges, Y. Sidis, H. F. Fong, L. P. Regnault, J. Bossy, A. Ivanov, and B. Keimer, Science **288**, 1234 (2000).

¹⁰ J. Brinkmann and P. A. Lee, Phys. Rev. Lett. **82**, 2915 (1999).

¹¹ A. Abanov and A. V. Chubukov, Phys. Rev. Lett. **83**, 1652 (1999); A. V. Chubukov and O. Tchernyshyov, unpublished.

¹² F. Onufrieva and P. Pfeuty, preprint cond-mat/9903097.
¹³ Y.-J. Kao, Q. Si, and K. Levin, Phys. Rev. B **61**, R11898 (2000).
¹⁴ M. R. Norman, Phys. Rev. B **61**, 14751 (2000).
¹⁵ J. Y. T. Wei, N.-C. Yeh, D. F. Garrigus, and M. Strasik, Phys. Rev. Lett. **81**, 2542 (1998).
¹⁶ S. M. Hayden, G. Aeppli, P. Dai, H. A. Mook, T. G. Perring, S.-W. Cheong, Z. Fisk, F. Dogan, and T. E. Mason, Physica B **241-243**, 765 (1998).
¹⁷ H. A. Mook, P. Dai, F. Dogan, and R. D. Hunt, Nature **404**, 729 (2000).

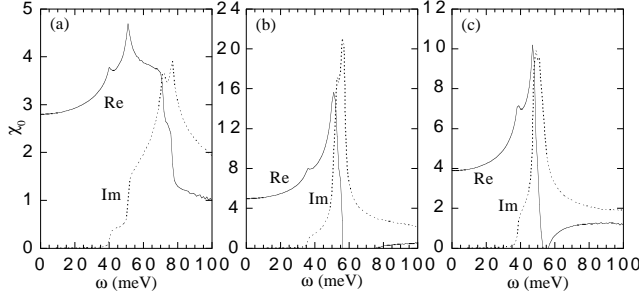


FIG. 1. $Re\chi_0$ and $Im\chi_0$ for $\vec{q} = (1, 0.8)\pi$ versus ω for the three dispersions of Table I, with $\Delta_{max}=29$ meV (a and b) and 25 meV (c), $\Gamma=0.5$ meV, and $T=13$ K. Units are states/eV/CuO plane, and so should be multiplied by $2\mu_B^2$ to compare to neutron susceptibilities.

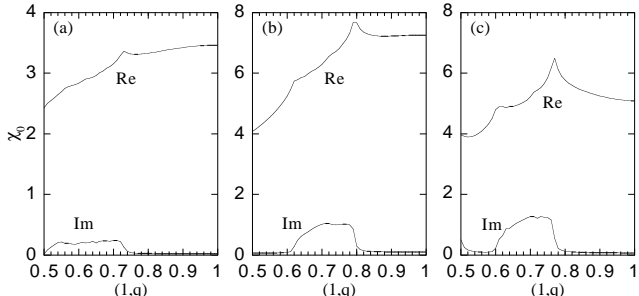


FIG. 2. $Re\chi_0$ and $Im\chi_0$ for $\omega=35$ meV versus $\vec{q} = (1, q_y)\pi$. Same notation as Fig. 1.

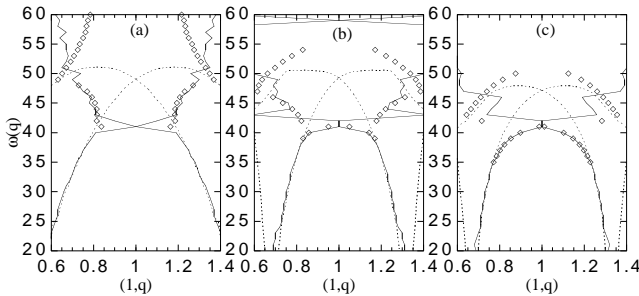


FIG. 3. $\vec{q} = (1, q_y)\pi$ where $Im\chi$ is maximal at a given ω (solid lines). The dashed lines are the spin gap energies, $\omega_g(\pm q)$, defined in the text, and the open diamonds represent the RPA pole condition, $1 - JRe\chi_0(q) = 0$. Same notation as Fig. 1, with $J=262$ meV (a), 111 meV (b), and 155 meV (c). Note that $Im\chi_0 \approx 0$ for ω below the lowest dashed line.

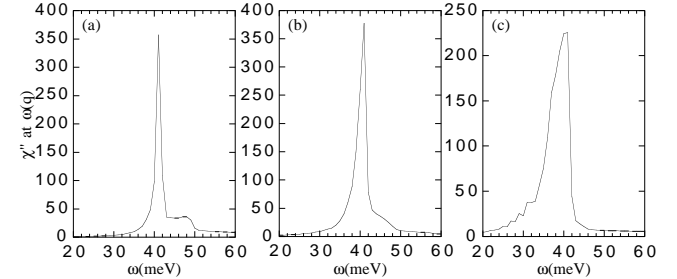


FIG. 4. Value of $Im\chi$ along the $\omega(q)$ dispersion relation from Fig. 3.

TABLE I. Tight binding dispersions based on angle resolved photoemission data. The first three columns list the coefficient, c_i , of each term (eV), that is $\epsilon(\vec{k}) = \sum c_i \eta_i(\vec{k})$, with tb1 and tb2 previously considered dispersions¹⁴, and tb3 a modified version of tb2 as discussed in the text. The last column lists the basis functions (the lattice constant a is set to unity).

tb1	tb2	tb3	$\eta_i(\vec{k})$
0.1305	0.0879	0.1197	1
-0.5951	-0.5547	-0.5881	$\frac{1}{2}(\cos k_x + \cos k_y)$
0.1636	0.1327	0.1461	$\cos k_x \cos k_y$
-0.0519	0.0132	0.0095	$\frac{1}{2}(\cos 2k_x + \cos 2k_y)$
-0.1117	-0.1849	-0.1298	$\frac{1}{2}(\cos 2k_x \cos k_y + \cos k_x \cos 2k_y)$
0.0510	0.0265	0.0069	$\cos 2k_x \cos 2k_y$